

# Stability of Surface Contacts for Humanoid Robots: Closed-Form Formulae of the Contact Wrench Cone for Rectangular Support Areas

Stéphane Caron<sup>1</sup>, Quang-Cuong Pham<sup>2</sup>, and Yoshihiko Nakamura<sup>1</sup>

<sup>1</sup>Department of Mechano-Informatics, The University of Tokyo, Japan

<sup>2</sup>School of Mechanical and Aerospace Engineering, Nanyang  
Technological University, Singapore

March 3, 2022

## Abstract

Humanoid robots locomote by making and breaking contacts with their environment. A crucial problem is therefore to find precise criteria for a given contact to remain stable or to break. For rigid surface contacts, the most general criterion is the Contact Wrench Condition (CWC). To check whether a motion satisfies the CWC, existing approaches take into account a large number of individual contact forces (for instance, one at each vertex of the support polygon), which is computationally costly and prevents the use of efficient inverse-dynamics methods. Here we argue that the CWC can be explicitly computed without reference to individual contact forces, and give closed-form formulae in the case of rectangular surfaces – which is of practical importance. It turns out that these formulae simply and naturally express three conditions: (i) Coulomb friction on the resultant force, (ii) ZMP inside the support area, and (iii) bounds on the yaw torque. Conditions (i) and (ii) are already known, but condition (iii) is, to the best of our knowledge, novel. It is also of particular interest for biped locomotion, where undesired foot yaw rotations are a known issue. We also show that our formulae yield simpler and faster computations than existing approaches for humanoid motions in single support, and demonstrate their consistency in the OpenHRP simulator.

## 1 Introduction

From the viewpoint of the robot, establishing contact with the environment amounts to constraining a certain number of Degrees Of Freedom (DOF) of an end-effector

link. For instance, a sliding planar contact imposes three *equality* constraints (two on the orientation of the link and one for the link-to-surface distance) while a fixed contact constraints all six DOFs of the end-effector link. A stability criterion can be seen as a set of *inequality* constraints describing the conditions under which these equalities are preserved.

The venerable Zero-Moment Point (ZMP) [1] criterion may be the best-known example of stability criterion for rigid surface contact. It is known [2] to be necessary but *not sufficient* for contact stability: in particular, it says nothing about possible sliding in the horizontal plane and rotation around the vertical axis (yaw). Yet, humanoid robots are often subject to significant yaw moments during single support phases, resulting in undesired foot rotations. Attesting the importance of this problem, recent works have been using upper-body motions to compensate for these yaws while continuing to use ZMP [3, 4].

A more principled (and general) way to address this problem is to consider *individual contact forces* distributed on the contact surface, as can be found *e.g.*, in bipedal balance control [5] and motion planning [6, 7]. This approach yields a stronger stability criterion than ZMP, and accounts for both the sliding and yaw rotation. It is however hampered by *redundancy*: the vector of contact forces has many more components (three times the number of contact points) than the degree of the contact constraint (six). This redundancy makes the resolution of the equations of motion fundamentally harder, as illustrated by the fact that state-of-the-art Inverse Dynamics based on QR-decomposition [8] only apply to non-redundant variables<sup>1</sup>. In Time-Optimal Path Parameterization (TOPP), redundancy prompted the use of further contact approximations [9] or expensive polytope projection algorithms [7]. In the present paper, we argue that such workarounds are no longer necessary if one uses the correct contact representation (for instance, both [9] and [7] boil down to a single matrix inversion for a biped in single-support, as we will see in Section 5).

The key insight here is that the condition that individual contact forces lie in their respective friction cones can be replaced by the condition that the *contact wrench* belongs to a certain *wrench cone* [10]. The contact wrench naturally solves the redundancy issue, as its dimension is minimal (six). It was advocated as a generalization of ZMP in [2], along with a stability theorem, and applied to walking pattern generation on rough terrains [11, 12]. However, this theorem makes the same “sufficient friction” assumption as ZMP, which means the resulting criterion does not account for sliding and yaw rotations. Besides, the contact wrench is

---

<sup>1</sup> When this is not the case, the authors advocate the use of Singular Value Decomposition to compute new independent variables; however, it is unclear how to compute the inequality constraints applying to these new variables.

computed from individual contact forces, which we argue yields unnecessarily extensive calculations: following [10], the wrench cone can be computed explicitly from the sole geometry of the contact surface.

In this paper, we derive the closed-form formulae of the wrench cone in the case of rectangular support areas, which is of practical importance since most humanoid robot feet can be adequately approximated by rectangles. This result helps simplify dynamics computations, as we will see for humanoid motions. It also provides an analytical description of “*yaw friction*”, from which we derive a simple and principled control law to prevent undesirable yaw rotations.

The rest of the paper is organized as follows. In Section 2, we recall the definitions related to contact stability. In Section 3, we discuss the physics of surface contact and give a theoretical justification for the practice of considering individual contact forces at the vertices of the contact polygon. Then, in Section 4, we derive a closed-form expression of the wrench cone in the case of rectangular contact areas. We apply the resulting solution in a humanoid experiment in Section 5 before concluding in Section 6.

## 2 Background

### 2.1 Contact Forces and Contact Wrench

Consider a robot with  $n$  degrees of freedom making  $N$  point contacts with the environment, at points  $C_1, \dots, C_N$  in the laboratory reference frame (RF). The equations of motion of the robot are:

$$\mathbf{M}(\mathbf{q})\ddot{\mathbf{q}} + \mathbf{h}(\mathbf{q}, \dot{\mathbf{q}}) = \mathbf{S}^\top \boldsymbol{\tau}_a + \sum_{i=1}^N \mathbf{J}(C_i)^\top \mathbf{f}_i, \quad (1)$$

where  $\mathbf{q}, \dot{\mathbf{q}}, \ddot{\mathbf{q}}$  are the  $n$ -dimensional vectors of DOF values, velocities and accelerations,  $\mathbf{M}$  is the  $n \times n$  inertia matrix,  $\mathbf{h}(\mathbf{q}, \dot{\mathbf{q}})$  the  $n$ -dimensional vector of gravity and Coriolis forces. In case the robot has  $n_a$  actuated joints,  $\boldsymbol{\tau}_a$  is the  $n_a$ -dimensional vector of torques at the actuated joints and  $\mathbf{S}$  is a  $n_a \times n$  joint selection matrix. Finally, for each  $i \in [1, N]$ ,  $\mathbf{f}_i$  is a 3-dimensional vector of contact force and  $\mathbf{J}(C_i)$  is the  $3 \times n$  *translation* Jacobian calculated at point  $C_i$ .

We assume that both the environment and the contacting link are rigid bodies. Thus, interactions between them can be represented by a single *contact wrench*

$\mathbf{W} = (\mathbf{f}, \boldsymbol{\tau})$ , which we can compute from contact forces as:

$$\mathbf{f} \stackrel{\text{def}}{=} \sum_i \mathbf{f}_i, \quad (2)$$

$$\boldsymbol{\tau} \stackrel{\text{def}}{=} \sum_i \overrightarrow{OC_i} \wedge \mathbf{f}_i, \quad (3)$$

where  $O$  is the origin of the link RF. The contact jacobian  $\mathbf{J}_{\text{wr}}$  is the  $6 \times n$  matrix obtained by stacking vertically  $\mathbf{J}(O)$ , the translation Jacobian computed at  $O$ , and  $\mathbf{J}_{\text{rot}}$ , the *rotation* Jacobian of the link, both taken with respect to the absolute RF. With these definitions, we have the following property:

$$\mathbf{J}_{\text{wr}}^\top \mathbf{W} = \sum_{i=1}^N \mathbf{J}(C_i)^\top \mathbf{f}_i. \quad (4)$$

(See Appendix A for a proof.) Then, the equations of motion can be rewritten as:

$$\mathbf{M}(\mathbf{q})\ddot{\mathbf{q}} + \mathbf{h}(\mathbf{q}, \dot{\mathbf{q}}) = \mathbf{S}^\top \boldsymbol{\tau}_a + \mathbf{J}_{\text{wr}}^\top \mathbf{W}. \quad (5)$$

## 2.2 Contact Stability

Assume now that the robot is in a given *state*  $(\mathbf{q}, \dot{\mathbf{q}})$ . The accelerations  $\ddot{\mathbf{q}}$  and generalized forces exerted on the robot (actuated torques or contact forces) are bound by a *complementarity* conditions [13]. For the sake of the explanation, let us consider first the simple case of a single translation coordinate  $x$ , as depicted in Figure 1.

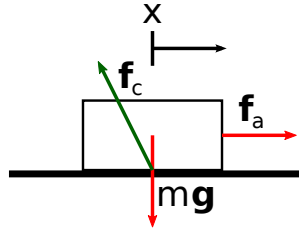


Figure 1: Block on a horizontal surface with one DOF.

Under Coulomb's friction model, either of the following situations occurs :

- **Fixed contact:**  $\ddot{x} = 0$  and the contact force obeys  $|f_c^t| \leq \mu f_c^n$ , where  $f_c^t$  and  $f_c^n$  are respectively the horizontal and vertical components of  $\mathbf{f}_c$  and  $\mu$  is the static friction coefficient;

- **Sliding contact:**  $\ddot{x} > 0$  and the contact force obeys  $f_c^t = -\mu_k f_c^n$ , where  $\mu_k$  is the kinetic friction coefficient.

The acceleration  $\ddot{x}$  and contact force  $\mathbf{f}_c$  are in a *complementary* relationship: when one is equality-constrained, the other is inequality-constrained. Similarly, for the general case of a 6-DOF end-effector in contact, the translational and rotational accelerations of the link are in a complementary relationship with some generalized contact forces  $\gamma$  (here,  $\gamma = \mathbf{W}$  or  $(\mathbf{f}_1, \dots, \mathbf{f}_N)$ ). The *contact mode* describes, for each variable in a complementary relationship, whether it is equality- or inequality-constrained. In contact stability, we are interested in the *fixed contact mode* where the position and orientation of the end-effector are equality-constrained to a reference value.

**Definition 1 (Weak Contact Stability)** *A contact is weakly stable when there exists a solution  $(\ddot{\mathbf{q}}, \tau_a, \gamma)$  of the equations of motion satisfying the fixed contact mode for all contacting links.*

That is to say,

- for each contact  $(i)$ , the relative velocity and acceleration at contact are zero:  $\mathbf{J}_{\text{wr}}^{(i)} \dot{\mathbf{q}} = 0$  and  $\mathbf{J}_{\text{wr}}^{(i)} \ddot{\mathbf{q}} = -\dot{\mathbf{J}}_{\text{wr}}^{(i)} \dot{\mathbf{q}}$ ,
- actuated torques  $\tau_a$  are within torque limits,
- complementary forces  $\gamma$  satisfy their inequality constraints (friction cones or wrench cone).

This formulation has been widely used in the literature. In approaches based on inverse dynamics, the conditions on  $(\dot{\mathbf{q}}, \ddot{\mathbf{q}})$  are first enforced kinematically, then torques and complementary forces are solved [7, 8].

The “weakness” in the definition above refers to the notions of strong and weak stability, as stated by [13]. Strong stability happens when *all* solutions to the equations of motion satisfy the fixed contact mode. Note that choosing between contact forces and the contact wrench changes the equations of motion (Equations (1) and (5), respectively), but the underlying contact stability is the same by Equation (4). In the rest of the paper, we will always refer to contact stability in the weak sense.

### 3 Surface Contact

Suppose we take contact forces  $\mathbf{f}_1, \dots, \mathbf{f}_N$  as complementary variables to the position and orientation of the contacting link. Let  $f_i^n$  and  $f_i^t$  denote the normal and

the tangential components of the contact force  $\mathbf{f}_i$ . Coulomb friction provides the complementary inequalities:

- **Unilaterality:**  $f_i^n > 0,$  (6)

- **Non-slippage:**  $\|\mathbf{f}_i^t\| \leq \mu f_i^n,$  (7)

where  $\mu$  is the static coefficient of friction.

However, when the contact is done through a surface and not through a set of points, the reality of contact is that of continuum mechanics. In this case, the action of the environment at the contact surface  $\mathcal{S}$  is described by two quantities: a scalar field  $p(x, y)$  corresponding to normal *pressure*, and a two-dimensional vector field  $\boldsymbol{\sigma}(x, y)$  for tangential mechanical *stress*. Figure 2-(A) illustrates these two fields for a rectangular contact area. For convenience, we also will denote by  $\boldsymbol{\nu} \stackrel{\text{def}}{=} \boldsymbol{\sigma}(x, y) + p(x, y)\mathbf{n}$ , where  $\mathbf{n}$  is the unit vector normal to the contact surface. The equations of motion become

$$\mathbf{M}\ddot{\mathbf{q}} + \mathbf{h} = \mathbf{S}^\top \boldsymbol{\tau}_a + \int_{\mathcal{S}} \mathbf{J}(C_{xy})^\top \boldsymbol{\nu}(x, y) dx dy \quad (8)$$

where  $\mathbf{J}(C_{xy})$  is the  $3 \times n$  translation Jacobian calculated at the point of coordinate  $C_{xy}$  on the surface (taken in the laboratory RF). The wrench resulting from  $\boldsymbol{\nu}(x, y)$  is

$$\mathbf{f} \stackrel{\text{def}}{=} \int_{\mathcal{S}} \boldsymbol{\nu}(x, y) dx dy, \quad (9)$$

$$\boldsymbol{\tau} \stackrel{\text{def}}{=} \int_{\mathcal{S}} \overrightarrow{OC_{xy}} \wedge \boldsymbol{\nu}(x, y) dx dy, \quad (10)$$

where  $O$  is the origin of the link RF. Under Coulomb friction, the inequality constraints for  $\boldsymbol{\nu}(x, y)$  are:

- **Unilaterality:**  $p(x, y) > 0,$  (11)

- **Non-slippage:**  $\|\boldsymbol{\sigma}(x, y)\| \leq \mu p(x, y).$  (12)

Note that taking a constant  $\mu$  in Equation (12) is an approximation: in reality, the friction coefficient  $\mu(x, y)$  varies with the position on the surface.

In the present literature, surface contact is often modeled using sets of contact points: sometimes more than required by positional constraints (*e.g.*, nearly 30 per contacting link in [7]) or one at each vertex of the convex hull (*e.g.*, in [5]). The proposition below gives a theoretical justification for the latter practice.

**Proposition 1** Assume that the contact surface  $\mathcal{S}$  is a convex polygon with vertices  $C_1, \dots, C_N$ . If there exists  $\boldsymbol{\nu}(x, y)_{(x, y) \in \mathcal{S}}$  satisfying complementary inequality constraints (11)-(12), then there will exist contact forces applied at  $C_1, \dots, C_N$  and summing up to the same contact wrench that satisfy complementary inequality constraints (6)-(7).

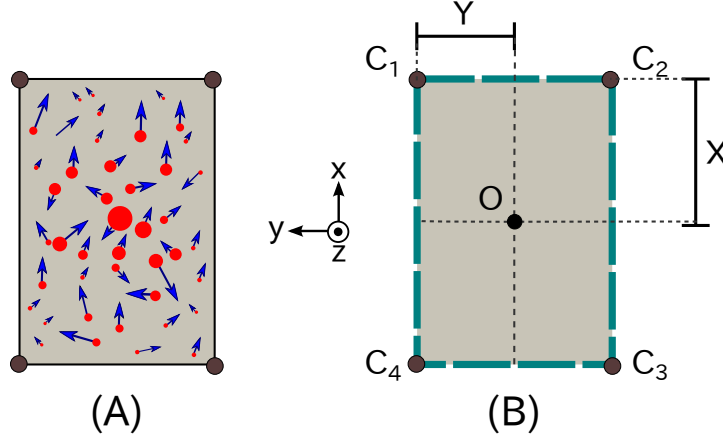


Figure 2: Contact in the surface plane. (A) Example of stress/pressure fields. Red discs indicate the magnitude of pressure by their size. Blue arrows show tangential stress. (B) Notations used in Section 4.

*Proof:* consider pressure and stress fields summing up to  $\mathbf{W}$ . By convexity, one can find strictly positive functions  $\alpha_1(x, y), \dots, \alpha_k(x, y)$  such that  $\sum_i \alpha_i(x, y) = 1$  and each point  $C_{xy} \in \mathcal{S}$  can be written  $C_{xy} = \sum_i \alpha_i(x, y) C_i$ . Then, define for each vertex  $C_i$  a force

$$\mathbf{f}_i := \int_{\mathcal{S}} \alpha_i(x, y) \boldsymbol{\nu}(x, y) dx dy,$$

By positivity of the  $\alpha_i$ 's, it is straightforward to check that all  $f_i^n > 0$  and  $\|\mathbf{f}_i^t\| \leq \mu f_i^n$ . In addition, this expression of  $\mathbf{f}_i$  ensures that the resulting wrenches are equal, i.e., (2) = (9) and (3) = (10).  $\square$

We furthermore argue that, when the friction coefficient  $\mu$  is assumed to be constant as in Equation (12), the two conditions are equivalent. The complete proof of this equivalence, which involves reconstructing pressure and stress fields given local and boundary conditions, is however out of the scope of this paper. The bottom line of this argument is that using contact forces at vertices of the convex hull completely describes the dynamics of surface contact. The wrench cone that we derive in the next section will share the same characteristic.

## 4 Wrench Cone for Rectangular Surfaces

Consider a rectangular area  $(C_1C_2C_3C_4)$  as depicted in Figure 2 (B). We calculate the contact wrench  $\mathbf{W}$  at the center  $O$  in the link's RF.<sup>2</sup> Let us denote by  $(f_i^x, f_i^y, f_i^z)$  the three components of the contact force at point  $C^i$ . Under the common linear approximation of friction cones, Coulomb inequalities become

$$|f_i^x|, |f_i^y| \leq \mu f_i^z \quad (13)$$

$$f_i^z > 0 \quad (14)$$

The wrench cone is then given by the following proposition.

**Proposition 2** *There exists a solution  $(\mathbf{f}_1, \dots, \mathbf{f}_4)$  satisfying inequalities (13)-(14) if and only if there exists a wrench  $\mathbf{W} = (f^x, f^y, f^z, \tau^x, \tau^y, \tau^z)$  such that:*

$$|f^x| \leq \mu f^z \quad (15)$$

$$|f^y| \leq \mu f^z \quad (16)$$

$$f^z > 0 \quad (17)$$

$$|\tau^x| \leq Y f^z \quad (18)$$

$$|\tau^y| \leq X f^z \quad (19)$$

$$\tau_{min} \leq \tau^z \leq \tau_{max} \quad (20)$$

where

$$\begin{aligned} \tau_{min} &\stackrel{\text{def}}{=} -\mu(X + Y)f^z + |Y f^x - \mu\tau^x| + |X f^y - \mu\tau^y|, \\ \tau_{max} &\stackrel{\text{def}}{=} +\mu(X + Y)f^z - |Y f^x + \mu\tau^x| - |X f^y + \mu\tau^y|. \end{aligned}$$

The proof of this proposition is given in Appendix A.1. The validity of this expression was also tested empirically with a script available at [14].

Let us now detail each line of the wrench cone. The first two inequalities (15)-(16) correspond to the usual Coulomb friction. Inequalities (17), (18) and (19) are equivalent to the ZMP condition. The last inequality (20) provides a bound on the admissible yaw torque that was implicitly encoded in the contact-force model. Note how this relation is more complex than a mere “no rotation occurs while  $\tau^z$  is small enough”, as it is coupled with all other components of the contact wrench. Notably, the “safest” value is not zero but:

$$\begin{aligned} \tau_{\text{safe}} &\stackrel{\text{def}}{=} (\tau_{min} + \tau_{max})/2 \\ &= \text{sgn}(-f^x\tau^x) \min(Y|f^x|, \mu|\tau^x|) \\ &\quad + \text{sgn}(-f^y\tau^y) \min(X|f^y|, \mu|\tau^y|), \end{aligned}$$

---

<sup>2</sup>multiply by the link's rotation matrix for a wrench in the absolute RF

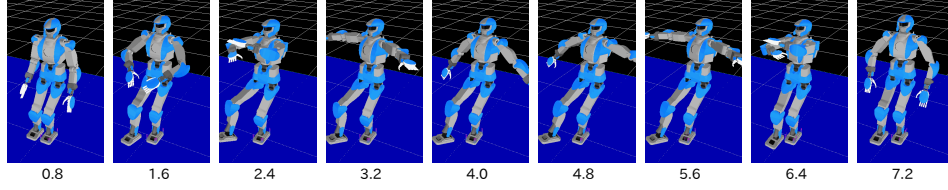


Figure 3: Snapshots of the retimed motion. The motion lasts 7.285 s. Time stamps are shown below each frame. This motion stresses all components of the wrench cone. The first part stresses the pitch by moving the COM forward. The second segment extends the arms, then keeps the left arm still while moving the right arm, thus stressing the roll. At the same time, the chest pitch is actuated back and forth, which stresses the yaw. Finally, the waist performs an elliptic motion (back and forth, up and down) throughout the whole motion, thus stressing the translation of the contact foot.

where  $\text{sgn}$  is the sign function. From (20),  $\tau^z$  may deviate from  $\tau_{\text{safe}}$  by at most

$$\mu(X + Y)f^z - \max(Y|f^x|, \mu|\tau^x|) - \max(X|f^y|, \mu|\tau^y|).$$

We see that higher tangential forces or roll-pitch torques reduce the range of admissible yaw torques. In particular, when these other constraints are saturated (for instance when the ZMP reaches a corner of the support polygon),  $\tau_{\text{safe}}$  is the *only solution* that prevents the contact from breaking. Therefore,  $\tau^z = \tau_{\text{safe}}$  appears as a sensible control law to prevent undesired yaw rotations.

## 5 Experiment

We test the validity of the Contact Wrench Condition (CWC) in the integrated simulator OpenHRP with a model of the HRP4 robot. Note that OpenHRP has its own contact model where forces are distributed along the edges (not corners) of the contact surface.

We implemented the CWC condition within the Time-Optimal Path Parameterization framework (TOPP), a well-known projection of system dynamics along a pre-defined path that has been used for motion planning of humanoid robots [7, 15, 9]. We considered the case of a single contact at the left foot and designed a motion that would challenge all six contact DOFs. In single contact, the contact wrench is fully determined by the unactuated rows of the equation of motion, *i.e.*,

$$\mathbf{W} = (\mathbf{P}\mathbf{J}_{\text{wr}})^{-1}\mathbf{P} [\mathbf{M}(\mathbf{q})\ddot{\mathbf{q}} + \mathbf{h}(\mathbf{q}, \dot{\mathbf{q}})]$$

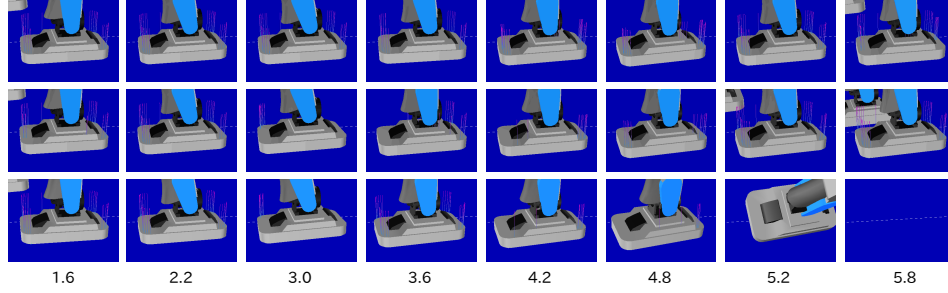


Figure 4: Zoom on the contact forces computed by OpenHRP at the left foot. The first row corresponds to the retimed motion (7.29 s), the second to the 10% uniform acceleration of the retimed motion (6.55 s) and the third to the 15% uniform acceleration (6.19 s). Time stamps are shown below each column. The retimed motion maintains surface contact with contact forces distributed all around the contact area, except between 4.2 and 4.8 s where they are mostly on the left half of the foot. The 10%-accelerated version goes to point contact (3.0 s) and line edge contact (3.6 to 4.8 s) but does not fall. At 15% acceleration, the CWC violation overcomes the stabilizer’s ability and the robot falls.

where  $\mathbf{P} = \mathbf{I} - \mathbf{S}$  is the unactuated line selection matrix. Note how computing the constraint projector is straightforward when using the contact wrench: it is not the case when contact forces are used, as we observed in previous research [9] (where we resolved the force redundancy with a force-binding model).

For this experiment, we designed by hand a set of eleven key postures. The geometric path was obtained by interpolating Bezier curves between these postures and applying a kinematic filter to fix the position and orientation of the support foot on the ground. To get a feasible trajectory from this path (*i.e.*, to compute the timing information) we used the open-source TOPP solver [16]. The solver takes as input the path and a vector representation of the system dynamics along it, which is easy to compute once one knows the projectors mentioned above (see [9] for details). Figure 3 shows a timelapse of the final retimed motion. Videos are also available online at [14].

An interesting thing to note about TOPP is that, because of time optimality, the retimed motion always saturates at least one of the contact constraints. In an ideal setting with perfect system dynamics, the obtained trajectory should therefore be at the limit of contact: it would execute correctly, but the contact would break as soon as one tries to perform the motion faster at any time instant. We observed this phenomenon in the experiment, as depicted in Figure 4.

There are, however, a few points to discuss. In order to ensure proper tracking

of the computed trajectory, we used HRP4’s stabilizer module, which occasionally changes the actual joint angles. In turn, this behavior violates the assumption made by TOPP that the robot follows a precise geometric path, and the constraints may get under- or over-saturated. To alleviate for this issue, we added safety margins in TOPP’s conditions: we scaled the contact area by 45% and set a smaller friction coefficient  $\mu = 0.4$  (versus  $\mu = 0.8$  in OpenHRP). Consequently, it was possible in practice to accelerate the retimed motion by about 5% (*i.e.*, reducing the total duration by 5% with uniform timescaling) and obtain a successful execution. However, we still observed the expected phenomenon with relatively small changes: for a 10% acceleration (by uniform timescaling), the humanoid started to lose surface contact, but the stabilizer was still able to recover; for a 15% acceleration, the violation of the contact constraint was too large and the robot fell. See Figure 4.

## 6 Conclusion

In this paper, we calculated the closed-form expression of the wrench cone for rectangular contact surfaces. This formula has several implications. First, it is very simple, making computations much easier than any previous formulation based on contact forces. Second, it describes concisely the phenomenon of *yaw friction* by a double-inequality that is, to the best of our knowledge, novel. From these bounds, we derived a simple control law to avoid undesired foot rotations, a recurring problem for bipeds in single contact. Finally, we showed how our criterion can give simpler and faster computations than contact forces for humanoid motions in single support, and demonstrated it with dynamic motions simulated in OpenHRP.

## References

- [1] M. Vukobratović and B. Borovac, “Zero-moment point—thirty five years of its life,” *International Journal of Humanoid Robotics*, vol. 1, no. 01, pp. 157–173, 2004.
- [2] H. Hirukawa, S. Hattori, K. Harada, S. Kajita, K. Kaneko, F. Kanehiro, K. Fujiwara, and M. Morisawa, “A universal stability criterion of the foot contact of legged robots—adios zmp,” in *Robotics and Automation, 2006. ICRA 2006. Proceedings 2006 IEEE International Conference on*. IEEE, 2006, pp. 1976–1983.
- [3] B. Ugurlu, J. A. Saglia, N. G. Tsagarakis, and D. G. Caldwell, “Yaw moment compensation for bipedal robots via intrinsic angular momentum constraint,” *International Journal of Humanoid Robotics*, vol. 9, no. 04, 2012.
- [4] R. Cisneros, K. Yokoi, and E. Yoshida, “Yaw moment compensation by using full body motion,” in *Mechatronics and Automation (ICMA), 2014 IEEE International Conference on*. IEEE, 2014, pp. 119–125.
- [5] C. Ott, M. A. Roa, and G. Hirzinger, “Posture and balance control for biped robots based on contact force optimization,” in *Humanoid Robots (Humanoids), 2011 11th IEEE-RAS International Conference on*. IEEE, 2011, pp. 26–33.

- [6] L. Saab, O. E. Ramos, F. Keith, N. Mansard, P. Soueres, and J. Fourquet, “Dynamic whole-body motion generation under rigid contacts and other unilateral constraints,” *Robotics, IEEE Transactions on*, vol. 29, no. 2, pp. 346–362, 2013.
- [7] K. Hauser, “Fast interpolation and time-optimization with contact,” *The International Journal of Robotics Research*, vol. 33, no. 9, pp. 1231–1250, 2014.
- [8] L. Righetti, J. Buchli, M. Mistry, M. Kalakrishnan, and S. Schaal, “Optimal distribution of contact forces with inverse-dynamics control,” *The International Journal of Robotics Research*, vol. 32, no. 3, pp. 280–298, 2013.
- [9] S. Caron, Y. Nakamura, and Q.-C. Pham, “Kinodynamic motion retiming for humanoid robots,” in *Proceedings of the 32nd Annual Conference of the Robotics Society of Japan*, 2014.
- [10] D. J. Balkcom and J. C. Trinkle, “Computing wrench cones for planar rigid body contact tasks,” *The International Journal of Robotics Research*, vol. 21, no. 12, pp. 1053–1066, 2002.
- [11] H. Hirukawa, S. Hattori, S. Kajita, K. Harada, K. Kaneko, F. Kanehiro, M. Morisawa, and S. Nakaoka, “A pattern generator of humanoid robots walking on a rough terrain,” in *Robotics and Automation, 2007 IEEE International Conference on*. IEEE, 2007, pp. 2181–2187.
- [12] Y. Zheng, M. C. Lin, D. Manocha, A. H. Adiwahono, and C.-M. Chew, “A walking pattern generator for biped robots on uneven terrains,” in *Intelligent Robots and Systems (IROS), 2010 IEEE/RSJ International Conference on*. IEEE, 2010, pp. 4483–4488.
- [13] J.-S. Pang and J. Trinkle, “Stability characterizations of rigid body contact problems with coulomb friction,” *ZAMM-Journal of Applied Mathematics and Mechanics/Zeitschrift für Angewandte Mathematik und Mechanik*, vol. 80, no. 10, pp. 643–663, 2000.
- [14] <https://scaron.info/research/conf/icra-2015.html>, 2014, [Online].
- [15] Q.-C. Pham, S. Caron, and Y. Nakamura, “Kinodynamic planning in the configuration space via admissible velocity propagation,” in *Robotics: Science and Systems*, 2013.
- [16] Q.-C. Pham, “A general, fast, and robust implementation of the time-optimal path parameterization algorithm,” *IEEE Transactions on Robotics (to appear)*, 2014. [Online]. Available: <http://arxiv.org/abs/1312.6533>

## A Proof of Equation 4

The rotation Jacobian satisfies  $\boldsymbol{\omega} = \mathbf{J}_{\text{rot}} \dot{\mathbf{q}}$ , where  $\boldsymbol{\omega}$  is the rotation velocity of the link. An interesting consequence of this property is that for any point  $C$  on the link and any vector  $\mathbf{u}$ , one has

$$\left( \frac{\partial \overrightarrow{OC}}{\partial \mathbf{q}} \right)^\top \mathbf{u} = \mathbf{J}_{\text{rot}}^\top \left( \overrightarrow{OC} \wedge \mathbf{u} \right). \quad (21)$$

Next, the position of any point  $C_i$  of the link in the absolute RF is related to that of its origin  $O$  by  $C_i = O + \overrightarrow{OC_i}$ . The corresponding translation Jacobian is  $\mathbf{J}(C_i) = \frac{\partial C_i}{\partial \mathbf{q}} = \mathbf{J}(O) + \frac{\partial \overrightarrow{OC_i}}{\partial \mathbf{q}}$ . Thus,

$$\sum_i \mathbf{J}(C_i)^\top \mathbf{f}_i = \mathbf{J}(O)^\top \sum_i \mathbf{f}_i + \sum_i \left( \frac{\partial \overrightarrow{OC_i}}{\partial \mathbf{q}} \right)^\top \mathbf{f}_i.$$

The first term of the expression equals the translation component of  $\mathbf{J}_{\text{wr}}^\top \mathbf{W}$ . By applying (21), we see that the second term equals  $\mathbf{J}_{\text{rot}}^\top (\overrightarrow{OC_i} \wedge \mathbf{f}_i)$ . Factoring  $\mathbf{J}_{\text{rot}}^\top$  out of the summation yields the rotation component of  $\mathbf{J}_{\text{wr}}^\top \mathbf{W}$ .  $\square$

## A.1 Calculation of the Wrench Cone

The wrench is defined by (2)-(3) as:

$$\begin{aligned} f^x &= f_1^x + f_2^x + f_3^x + f_4^x \\ f^y &= f_1^y + f_2^y + f_3^y + f_4^y \\ f^z &= f_1^z + f_2^z + f_3^z + f_4^z \\ \tau^x &= Y(f_1^z - f_2^z - f_3^z + f_4^z) \\ \tau^y &= -X(f_1^z + f_2^z - f_3^z - f_4^z) \\ \tau^z &= X(f_1^y + f_2^y - f_3^y - f_4^y) - Y(f_1^x - f_2^x - f_3^x + f_4^x). \end{aligned}$$

By unilaterality (14) we have  $f^z > 0$ , so we can define:

$$\begin{aligned} K_1 &:= f^x / \mu f^z & C_1 &:= \tau^x / Y f^z \\ K_2 &:= f^y / \mu f^z & C_2 &:= \tau^y / X f^z \\ K_3 &:= \tau^z / \mu (X + Y) f^z & D_i &:= f_i^z / \sum_i f_i^z \\ p_x &:= X / (X + Y) & p_y &:= Y / (X + Y) \\ \alpha_i^x &:= f_i^x / \mu f_i^z & \alpha_i^y &:= f_i^y / \mu f_i^z \end{aligned}$$

and normalize the system by dividing each row accordingly. From the non-slippage constraint (13), we have  $\alpha_i^x, \alpha_i^y$  and  $D_i \in [-1, 1]$ . Then, introduce the new variables:

$$\begin{aligned} \gamma_x &= \alpha_1^x D_1 + \alpha_4^x D_4 & \gamma'_x &= \alpha_2^x D_2 + \alpha_3^x D_3 \\ \gamma_y &= \alpha_1^y D_1 + \alpha_2^y D_2 & \gamma'_y &= \alpha_3^y D_3 + \alpha_4^y D_4 \end{aligned}$$

We can reduce the complete system in two ways. First, using the fact that the relation  $\mathbf{M}$  from  $\alpha$  to  $\gamma$  is a linear surjection from  $[-1, 1]^8$  to  $\mathbf{M}[-1, 1]^8 = \{|\gamma_i^{x|y}| \leq D_j + D_k\}$  (the computation of antecedents being straightforward). Since there is no other constraint on the  $\alpha_i$ 's than their domain and relation to  $\gamma_i$ 's, one can obtain an equivalent system by replacing  $\alpha \in [-1, 1]^8$  by  $\gamma \in \mathbf{M}[-1, 1]^8$ . Then, the three equations in  $D_i$ 's are:

$$\begin{aligned} 1 &= D_1 + D_2 + D_3 + D_4, \\ C_1 &= D_1 - D_2 - D_3 + D_4, \\ C_2 &= -D_1 - D_2 + D_3 + D_4, \end{aligned}$$

By linear combination, we can use them to rewrite  $\mathbf{M}[-1, 1]^8$  as:  $2|\gamma_x| \leq 1 + C_1$ ,  $2|\gamma'_x| \leq 1 - C_1$ ,  $2|\gamma_y| \leq 1 - C_2$ ,  $2|\gamma'_y| \leq 1 + C_2$ . Finally, using the same equations,

one can express all  $D_i$ 's as functions of, *e.g.*,  $D_4$ . The inequalities  $\mathbf{D} \in [0, 1]^4$  become:

$$\begin{array}{rclcl} -1 + C_1 & \leq & 2D_4 & \leq & 1 + C_1 \\ C_1 + C_2 & \leq & 2D_4 & \leq & 2 + C_1 + C_2 \\ -1 + C_2 & \leq & 2D_4 & \leq & 1 + C_2 \\ 0 & \leq & 2D_4 & \leq & 2 \end{array}$$

This system has solutions if and only if all lower bounds are smaller than all upper bounds. Matching all pairs of lower and upper bounds one by one (we will show an example of this technique below in a more complex situation), one can check that all these inequalities boil down to  $C_1 \in [-1, 1]$  and  $C_2 \in [-1, 1]$ . The complete system is now:

$$\begin{array}{rcll} K_1 & = & \gamma_x + \gamma'_x & K_2 = \gamma_y + \gamma'_y \\ K_3 & = & p_x(\gamma_y - \gamma'_y) - p_y(\gamma_x - \gamma'_x) & \\ 2|\gamma_x| & \leq & 1 + C_1 & 2|\gamma'_x| \leq 1 - C_1 \\ 2|\gamma_y| & \leq & 1 - C_2 & 2|\gamma'_y| \leq 1 + C_2 \end{array}$$

And  $(C_1, C_2) \in [-1, 1]^2$ . One can use the first three equations to eliminate the redundant variables  $\gamma'_x$ ,  $\gamma_y$  and  $\gamma'_y$ , expressing them as functions of  $\gamma_x$  in the inequality constraints. After simplification, the resulting system is:

$$2p_y\gamma_x \leq p_y(1 + C_1) \tag{22}$$

$$2p_y\gamma_x \leq p_y(1 - C_1) + 2p_yK_1 \tag{23}$$

$$2p_y\gamma_x \leq p_x(1 - C_2) - K_3 + p_yK_1 - p_xK_2 \tag{24}$$

$$2p_y\gamma_x \leq p_x(1 + C_2) - K_3 + p_yK_1 + p_xK_2 \tag{25}$$

$$2p_y\gamma_x \geq -p_y(1 + C_1) \tag{26}$$

$$2p_y\gamma_x \geq -p_y(1 - C_1) + 2p_yK_1 \tag{27}$$

$$2p_y\gamma_x \geq -p_x(1 - C_2) - K_3 + p_yK_1 - p_xK_2 \tag{28}$$

$$2p_y\gamma_x \geq -p_x(1 + C_2) - K_3 + p_yK_1 + p_xK_2 \tag{29}$$

And  $(C_1, C_2) \in [-1, 1]^2$ . There exist a solution  $\gamma_x$  if and only if all of its lower bounds are smaller than all of its upper bounds. Let us match all pairs of lower bounds (26)-(29) and upper bounds (22)-(25). One can check that:

- $(26) \leq (22) \Leftrightarrow C_1 \geq -1$
- $(26) \leq (23) \Leftrightarrow K_1 \geq -1$
- $(26) \leq (24) \Leftrightarrow K_3 - p_yK_1 + p_xK_2 - p_yC_1 + p_xC_2 \leq 1$
- $(26) \leq (25) \Leftrightarrow K_3 - p_yK_1 - p_xK_2 - p_yC_1 - p_xC_2 \leq 1$

- $(27) \leq (22) \Leftrightarrow K_1 \leq 1$
- $(27) \leq (23) \Leftrightarrow C_1 \leq 1$
- $(27) \leq (24) \Leftrightarrow K_3 + p_y K_1 + p_x K_2 + p_y C_1 + p_x C_2 \leq 1$
- $(27) \leq (25) \Leftrightarrow K_3 + p_y K_1 - p_x K_2 + p_y C_1 - p_x C_2 \leq 1$
- $(28) \leq (22) \Leftrightarrow -K_3 + p_y K_1 - p_x K_2 - p_y C_1 + p_x C_2 \leq 1$
- $(28) \leq (23) \Leftrightarrow -K_3 - p_y K_1 - p_x K_2 + p_y C_1 + p_x C_2 \leq 1$
- $(28) \leq (24) \Leftrightarrow C_2 \leq 1$
- $(28) \leq (25) \Leftrightarrow K_2 \geq -1$
- $(29) \leq (22) \Leftrightarrow -K_3 + p_y K_1 + p_x K_2 - p_y C_1 - p_x C_2 \leq 1$
- $(29) \leq (23) \Leftrightarrow -K_3 - p_y K_1 + p_x K_2 + p_y C_1 - p_x C_2 \leq 1$
- $(29) \leq (24) \Leftrightarrow K_2 \leq 1$
- $(29) \leq (25) \Leftrightarrow C_2 \geq -1$

Consequently, the complete system becomes:

$$\begin{aligned}
K_3 &\leq 1 - p_y K_1 - p_x K_2 - p_y C_1 - p_x C_2 \\
K_3 &\leq 1 - p_y K_1 + p_x K_2 - p_y C_1 + p_x C_2 \\
K_3 &\leq 1 + p_y K_1 - p_x K_2 + p_y C_1 - p_x C_2 \\
K_3 &\leq 1 + p_y K_1 + p_x K_2 + p_y C_1 + p_x C_2 \\
K_3 &\geq -1 + p_y K_1 + p_x K_2 - p_y C_1 - p_x C_2 \\
K_3 &\geq -1 + p_y K_1 - p_x K_2 - p_y C_1 + p_x C_2 \\
K_3 &\geq -1 - p_y K_1 + p_x K_2 + p_y C_1 - p_x C_2 \\
K_3 &\geq -1 - p_y K_1 - p_x K_2 + p_y C_1 + p_x C_2
\end{aligned}$$

And  $(K_1, K_2, C_1, C_2) \in [-1, 1]^4$ . In a more concise form, these last eight inequalities can be written  $K_3 \geq -1 + p_y|K_1 - C_1| + p_x|K_2 - C_2|$  and  $K_3 \leq +1 - p_y|K_1 + C_1| - p_x|K_2 + C_2|$ . We conclude by de-normalizing all inequalities.  $\square$